Starch Fractions as Examples for Nonrandomly Branched Macromolecules. 3. Angular Dependence in Static Light Scattering

Gabriela Galinsky and Walther Burchard*

Institute of Macromolecular Chemistry, University of Freiburg, Sonnenstrasse 5, D-79104 Freiburg, Germany

Received December 3, 1996; Revised Manuscript Received March 24, 1997[⊗]

ABSTRACT: The angular dependences of seven degraded potato starch samples were measured by static light scattering in the dilute and semidilute regimes and analyzed on the basis of a previously treated model that resembles hyperbranched structures. These nonrandomly branched samples show only very limited intermediate range power law behavior and are not fractals. Furthermore the various samples of different molar masses are not self-similar to each other, but each sample exhibits its own exponent in the asymptotic region. These findings are in principle agreement with the predictions for the above-mentioned model that, however, neglects excluded volume effects. This fact causes a change in the meaning of the structure-determining parameter C of the model. The scattering curves from the semidilute regime could be condensed to one master curve when plotted against $qR_{app}(c)$, where $R_{app}(c)$ is the apparent radius of gyration and $q = (4\pi/\lambda)\sin(\theta/2)$ is the magnitude of the scattering vector with θ being the scattering angle. This master curve coincides with the particle scattering factor at zero concentration. No change in the shape of the macromolecules as a result of the osmotic force is deduced from this behavior. However association becomes effective when the overlap concentration is exceeded, which is recognized by a strong increase of $R_{g,app}(c)$ and pronounced deviations from the master curve of the angular dependence. A decrease of $R_{g,app}(c)$ as c^{-1} was predicted from scaling arguments, and up to $c = 5c^*$ *this prediction was fulfilled.*

Introduction

In two previous papers[1,2] we reported the global structure parameters of starch fractions from potato starch in 0.5 N NaOH solution and the concentration dependence of the inverse osmotic compressibility that was called the osmotic modulus. The global structure is defined by parameters which describe averages over the entire particle including thermodynamic and hydrodynamic interactions. These properties are based on three quantities, i.e. radius, volume, and molar mass of the particles. Typical examples are the radius of gyration R_g and the hydrodynamic radius R_h, where the latter is obtained from the Stokes−Einstein relationship *at infinite dilution*. Two other quantities, i.e. the second virial coefficient A_2 and the intrinsic viscosity (or viscosity number) $[\eta]$, are based on the ratio of the particle volume to the molar mass.

In a good solvent the reduced osmotic modulus $(M_w/RT)(\partial\pi/\partial c)$ describes the repulsive interactions among the particles. Both the global structure parameters and the reduced osmotic modulus are based on the *overall* structure that is "seen" in light-scattering experiments at small qR_g values, i.e. small scattering angles or at $\theta = 0$, respectively, where $q = (4\pi/\lambda)\sin(\theta/2)$ is the magnitude of the scattering vector with $\lambda = \lambda_0/n_0$ the wavelength of the light in a solvent of refractive index n_0 and θ the scattering angle; R_g is the radius of gyration. In two consecutive papers (parts 3 and 4) we now extend the investigation to the properties of the *internal structure* and *internal flexibility*. The internal structure can be studied by light-scattering experiments when $qR_g > 3$. In this range of the angular dependence of the scattered light, the "window" of detection is sufficiently narrow such that only short sections of the macromolecule are seen corresponding to distances $r_{ij} < R_g$ but still considerable larger than one Kuhn segment in length. The region of the internal structure and its mobility have to be distinguished from the *local* structure and mobility, which no longer follow Gaussian statistics even in the unperturbed state.

We studied first the internal structure and dynamics at infinite dilution. Then the region was extended to concentrations beyond the overlap concentration $c^* \equiv (A_2M_w)^{-1}$.[2] In that region the repulsion among the particles modifies all measurable quantities, and only apparent molar masses $M_{app}(c)$, radii of gyration $R_{g,app}(c)$, or hydrodynamic radii $R_{h,app}(c)$ are obtained, if the measurements are evaluated in the same manner as is common for systems at infinite dilution. In paper 2[2] we demonstrated how the apparent molar mass $M_{app}(c) \equiv RT(\partial c/\partial\pi)$ is affected by the concentration and the branched structure. We now try to describe the whole scattering behavior, i.e. the concentration *and* angular dependencies, in a scaled form. We consider this attempt as relevant, since scaling behavior can be expected for nonassociating systems; but this scaling will be violated when association or aggregation becomes effective. The present paper is confined to the static light-scattering results. The results obtained by dynamic light scattering are treated in a subsequent paper (paper 4).

As was already pointed out by Flory,[3] the amylopectin macromolecule as well as glycogen can be considered as a result of statistical but nonrandom polycondensation of $A\langle^{C}_{B}$-type monomers. (Flory's notation is $A\langle^{B_2}_{B_1}$). This polycondensation is a special case of the AB_2 polycondensation that leads to so-called hyperbranched materials. The glucose units in amylopectin differ from the common hyperbranching monomers solely by the fact that the reactivity of the functional C-group (the OH-group in the C_6 position of the glucose ring) is much lower than that of the B-group (the OH in the C_4 position). See the Appendix. In contrast to randomly branched materials the hyperbranched samples can never undergo covalent gelation. This is a property of

[⊗] Abstract published in *Advance ACS Abstracts,* July 1, 1997.

S0024-9297(96)01775-5 CCC: $14.00

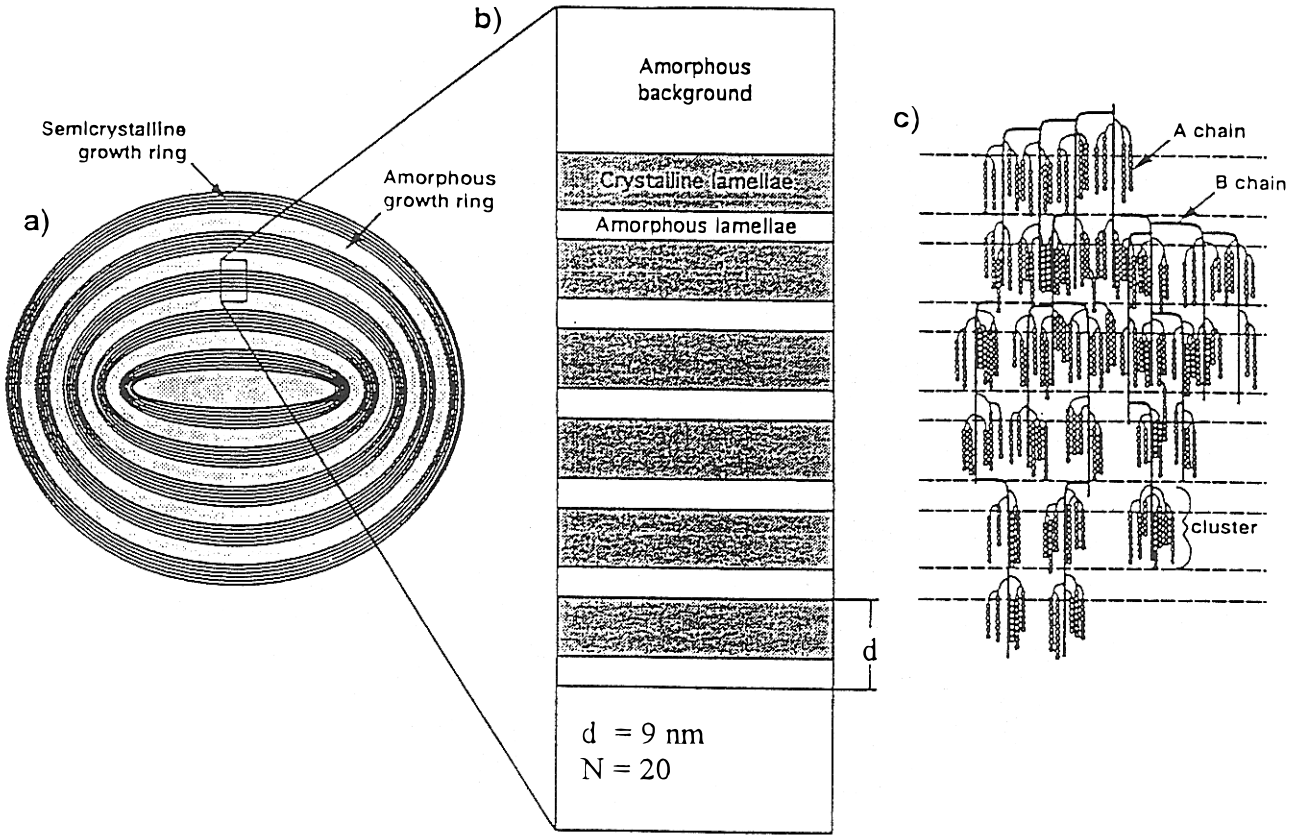

Figure 1. Model of the semicrystalline structure of starch granules:[7] (a) onion-like layers of amorphous (white) and semicrystalline domains; (b) schematic representation of the lamellar construction in the semicrystalline domain; (c) molecular arrangement of amylopectin in the lamellae according to Robin et al.[5]

the functional group in the A-position (the reducing end group of the glucose) that can react with group B or C only. Measurements of the already mentioned global parameters R_g, R_h, M_w/M_n, A_2, and $[\eta]$ of the starch fractions gave strong evidence for the validity of this model.[1]

The present contribution follows the question to which extent also the *internal* structure is correctly described by the $A\text{-}\{^{C}_{B}$ model. So far the theoretical model neglects excluded volume effects and the heterogeneity in branching that was disclosed by specific enzymatic degradation techniques of amylopectin.[4,5] It appeared of interest to look at what influence excluded volume and branching heterogeneity have on the structural parameters.

Experimental Section

The starch fractions were prepared by a controlled acid degradation of potato starch granules under conditions where the semicrystalline morphology of the granule is not affected.[1] This degradation technique, which was recently explored in detail by Fox and Robyt,[6] causes cleavage of the glycoside bonds only in the amorphous interlamellar sheets of the semicrystalline granules that are formed by the branching regions. Exploiting this particular morphology, which is schematically shown in Figure 1,[7,8] the acid degradation resulted in fractions which retained all essential features of the native amylopectin.[1] The long amylose chains, on the other hand, became preferentially degraded. These short chains did not significantly contribute to the scattering behavior compared to the much larger molar masses of the amylopectin fractions.

Fourteen fractions were prepared from potato starch granules by an acid degradation in methanolic or longer chain alcohol suspensions at room temperature,[1] but only seven of them had dimensions large enough to cause an angular dependence of the scattered light. This well-known degradation technique, which was recently optimized,[6] is often called linterization,[3] and therefore the different fractions are labeled as LDX, where LD stands for linterized dextrin and *X* for the fraction number. The details of the preparation were given in paper 1, where all results of the molecular characterization are reported.

Static light-scattering measurements were performed first with a modified and fully computerized SOFICA photogoniometer (G. Baur, Instrumentenbau, Hausen, Germany). The goniometers were equipped with a 2 mW HeNe laser ($\lambda_0 = 632$ nm) or a 5 mW Ar laser ($\lambda_0 = 488$ nm). The lasers were products of Uniphase. Measurements were made in an angular range of 30° to 145° in steps of 5°. The solvent was 0.5 N NaOH, and the concentration ranged from very dilute to 21% (w/v) solutions. The temperature was 20 °C, and a refractive index increment of $dn/dc = 0.142$ was used. All calibrations were made with the data given previously.[9]

All solutions were filtered three times through Millipore filters of 1.2, 0.8, 0.45, and 0.2 μm pore size respectively, depending on the molar mass of the samples, and the third time they were filtered directly into cylindrical light-scattering cells 0.8 cm in diameter. The cells were rinsed before use by freshly distilled acetone in a special rinsing apparatus to remove possibly adhered dust particles.

Results and Discussion

Dilute Solutions. *Results.* Only 7 of the prepared 14 fractions were chosen in this study, since the remaining fractions had molar masses below 400 000 g/mol and radii of gyration smaller than 24 nm. They exhibited no structure specific angular dependencies of the scattered light. Table 1 gives a list of some relevant parameters.

Figure 2 shows the double logarithmic plot of $R_\theta/(Kc)_{at\ c=0}$ as a function of the scattering vector $q =$

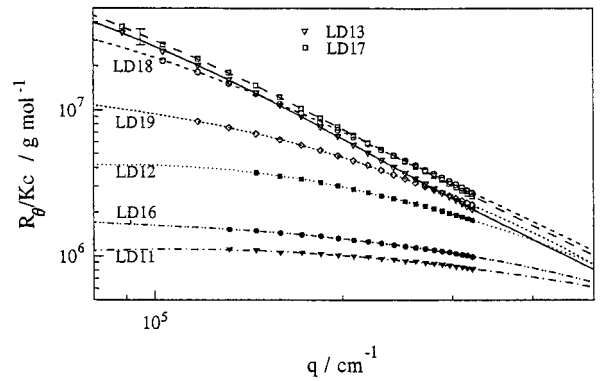

Figure 2. Double logarithmic plot of the scattering intensity R_θ/K as a function of $q = (4\pi n_0/\lambda_0) \sin \theta/2$ for seven degraded starch samples.

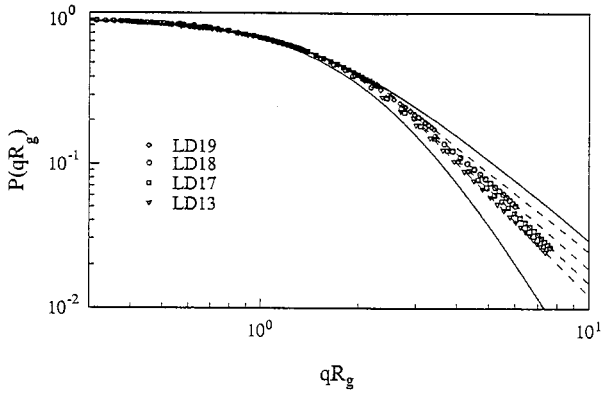

Figure 3. Same data as in Figure 2 but now plotted as $P(q) = S(q)/S(0)$ versus qR_g. The full lines correspond to the limiting cases of $C = 1$ (linear chains) and $C = 0$ (homogeneously branched).[13] See eq 1.

Table 1. Some Molecular Parameters of Degraded Starch Samples

sample	$10^{-6}M_w$ (g/mol)	R_g (nm)	10^4A_2 ((mol cm^3)/g^2)	R_h (nm)
LD11	0.92	36	1.00	27
LD16	1.87	48	0.60	35
LD12	5.20	70	0.28	61.5
LD19	14.5	113	0.13	84
LD18	43	180	0.082	150
LD17	64	190	0.060	215
LD13	97	233	0.025	228

$(4\pi n_0/\lambda_0) \sin(\theta/2)$. Figure 3 shows the same data, but now normalized with respect to the scattering intensity $R_{\theta=0}$ at $q = 0$. Both the particle scattering factor $P(qR_g) \equiv R_\theta/R_{\theta=0}$ and the values of the abscissa, qR_g, are dimensionless quantities. Therefore, in this scaled form the plot of Figure 3 has the character of a certain universality: Such curves depend no longer explicitly on the molar mass and the radius of gyration, if samples of self-similar structures are present. Self-similarity is given when the structure of a smaller sample is artificially expanded to the size of a large particle and both structures cannot be distinguished in their statistics. Also the representation of the structure in its Fourier transform (light scattering) must be universal. Such scaling behavior has indeed been observed with linear chain molecules and with randomly branched samples.[10] Up to values of $qR_g = 2$ also, the scattering data from the amylopectins in Figure 3 form one common curve, but at larger values systematic deviations occurred. Evidently the various samples do not fulfill the condition of self-similarity. Nonetheless, the various curves seem to approach power law behavior at large qR_g (often taken as a criterion for self-similarity[11]). The negative exponent usually represents the *ensemble* fractal dimension,[12] $\langle d_f \rangle$, of the nonfractionated system, but see the discussion below. The estimated slopes are listed in Table 2 together with a few other parameters to be discussed later in this contribution.

Table 2. Values of the *C*-parameter and Experimentally Determined Slopes of the Curves in Figure 3 in Comparison with the Theoretical Slopes at $qR_g = 8$ and with the Maximum Value

sample	$10^{-6}M_w$ (g/mol)	C (eq 1)	exp slope	theor slope at $qR_g = 8$[a]	max. theor slope[b]
LD12	5.2	0.50		−1.93	−2.00
LD19	14.5	0.33	−1.85	−1.98	−2.00
LD18	43	0.215	−2.02	−2.07	−2.08
LD17	64	0.155	−2.19	−2.15	−2.20
LD13	97	0.115	−2.32	−2.28	−2.32

[a] $d_{f,e} = 2.50 \pm 0.15$ from $M_w \propto R_g^{df,e}$. [b] $d_{f,e} = 2.15 \pm 0.15$ from $M_w \propto R_h^{df,e}$.

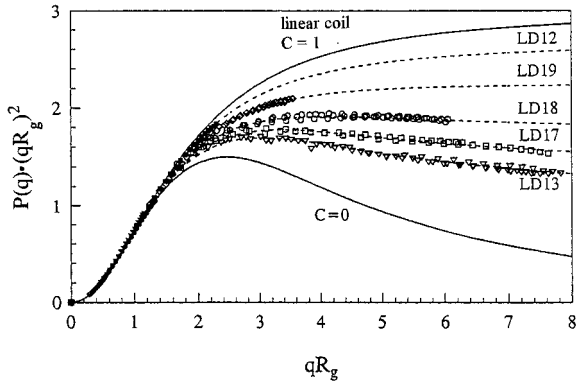

Figure 4. Kratky plot of the scattering data in Figure 3.

The difference in behavior is even better displayed in a Kratky plot (Figure 4) of the same data as shown in Figure 3. In such a plot the asymptotic region of large qR_g is emphasized and in a sense amplified by a multiplication of the scattering intensity with $(qR_g)^2$. The curves of Figure 4 could quantitatively be well described by the following equation for the particle scattering factor[13]

$$P(q) = \frac{1 + (C/3)(qR_g)^2}{[1 + ((1 + C)/6)(qR_g)^2]^2} \qquad (1)$$

This equation was previously derived for the A-$\langle^C_B$ polycondensation model, neglecting the influence of excluded volume.[13] The parameter C in eq 1 increases with the molar mass and is related to the branching probability p by an equation that is given in the Appendix together with other relationships for the A-$\langle^C_B$ model. The C-parameters obtained from the fit of the scattering data with eq 1 are listed in Table 2. Figure 5 shows the plot of these data against the molar mass M_w. The curve could be fitted with a branching probability of $p_{LS} = 5 \times 10^{-5}$ with an error of approximately 20%. This value is considerably smaller than $p = 0.04-0.05$, which was found from elemental analysis of permethylated amylopectin.[4] The value $p_P = 0.016$ was obtained from the molar mass dependence of the polydispersity ratio M_w/M_n,[1] and from the shrinking factor g_{R_g} the deduced value was $p_g = 0.026 \pm 0.001$.[1] (The subscripts *LS*, *P*, and *g* indicate the procedure of determining the branching probability.) The shrinking factor $g_{R_g} \equiv (R_{g,b}/R_{g,lin})^2$ is defined as the ratio of the two radii at the *same molar*

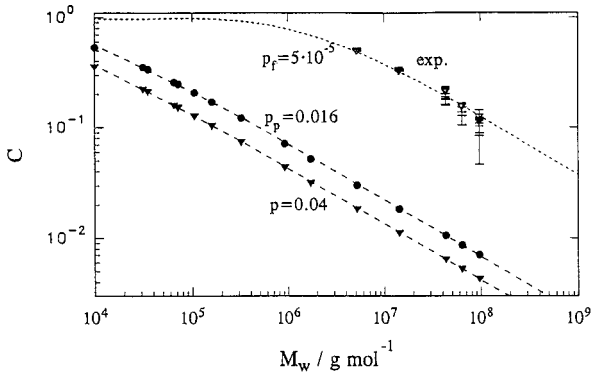

Figure 5. Plot of the *C*-parameters in eq 1 according to the A-$\langle^C_B$ polycondensation model[13] for branching probabilities of $p = 0.04$, $p_p = 0.016$, and $p_{LS} = 5 \times 10^{-5}$ compared with the experimentally observed *C*-parameters (symbols).

mass. A branched macromolecule has evidently smaller dimensions than a linear chain of the same molar mass, and due to theory[14] the decrease in g_{R_g} is a measure of the number of branches per molecule.

The amazingly strong variation in the branching density determined by different techniques calls for an explanation. An attempt is made in the next section. It will be followed by comments on the ensemble fractal behavior.

Meaning of the Various Branching Parameters. The large deviations in the four branching probabilities strikingly demonstrate some inconsistencies of the simple A-$\langle^C_B$-polycondensation model when applied to amylopectin. Clearly the value of $p = 0.040 \pm 0.005$, derived from the ratio of branching units to all anhydroglucose units, is the correct branching density.[4,15] The other values are based on structural assumptions. These can give the same values only if the made idealization is close to the real system. As already mentioned, the A-$\langle^C_B$ is incorrect in two aspects: the one is the disclosed heterogeneity in branching and the other is the neglected effect of excluded volume. These two main reasons will be discussed separately.

Influence of Branching Heterogeneity. The much lower value of $p_P = 0.016$ found from the molar mass dependence of the *polydispersity ratio* may have a rough explanation in the heterogeneity of branching that was first discovered by Robin, Mercier, and co-workers.[5] These authors concluded from a set of well designed enzymatic degradation experiments that densely branched clusters of about nine branching points are connected via longer internal, so-called B-chains. In a subsequent light-scattering study with a β-limiting dextrin (obtained by the action of β-amylase that cleaves maltose units from the chain ends), Thurn and Burchard[16] confirmed the model but concluded from a detailed quantitative analysis that only 4−5 chains are outgoing from the dense clusters. Since these chains are grafted onto very small nodules, the amylopectin structure may be considered as being constructed by end-linking of short-arm star-molecules with 4−5 arms, where still the reducing end has to be distinguished from the nonreducing end groups. In the densely branched nodules the 4−5 arms of these nodules have an effect of three armed nodules. The true branching density must be larger, intuitively by a factor $4.5/3.0 = 1.5$, resulting in a value of $p_P = 0.024 \pm 0.004$, which is somewhat closer to the value of the elemental analysis but still too low.[5,15]

The result of the *shrinking factors*, g_{R_g}, was described already in paper 1. The fit was made there with a slightly incorrect function for the shrinking factor. The correct relationship reads

$$g_{R_g} = \frac{6(1 + 2B_w)^{1/2}}{[1 + (1 + 2B_w)^{1/2}]^2} \tag{2}$$

with

$$B_w = p(1 - p)DP_w \tag{3}$$

which has to replace eq 8 of paper 1.[18] The fit with the corrected relationship gives $p_g = 0.026 \pm 0.001$, which again is lower than the branching probability p determined by elemental analysis. The reason for this deviation is based partially on the assumption of three-arm star repeating units but it can also be explained qualitatively on the basis of the Daoud−Cotton[19,20] model for star branched macromolecules. Due to the finite volume of the individual monomers, near the center of a branching unit (star center) a density overcrowding occurs that causes a stretching out of the chains. This effect increases with $f^{1/2}$, where f is the functionality of the branching point (number of arms), which in the present case is $f = 4.5$. Hence the outgoing linear chains, connecting two branching points, have a slightly larger end-to-end distance than the corresponding free linear chain. This reduces the shrinking and results in an apparent lower branching probability.

Effect of Excluded Volume. The apparent branching probability $p_{LS} =$ ca. 5×10^{-5} derived from the angular dependence of the scattered light is strikingly lower than the other ones. This is very likely an excluded volume effect. The positive values of the second virial coefficients A_2 prove the 0.5 N NaOH solution as a thermodynamically good solvent, and excluded volume must be effective. In their theoretical considerations Daoud and Cotton[19] showed that the excluded volume effect will be completely screened in branched materials if the chains are short. Gaussian behavior is expected but with a larger characteristic ratio because of segment overcrowding in the vicinity of the branching point. In amylopectin the interconnecting chains (B-chains) have only a length of approximately 20 anhydroglucose units, such that for the inner part of the amylopectin molecules the excluded volume effect will probably be small. This may be the reason why in the accessible q-regime of light scattering the particle scattering factors could be described by the A-$\langle^C_B$ model (eq 11), although the excluded volume effect is neglected there. The situation changes, however, when the shells at the outside are considered. These consist mainly of outer chains (non-branched A-chains) which are linked to the branched nodules of the macromolecule only via their reducing ends. In this periphery of the macromolecule the excluded volume can now become effective.[19] It will decrease the fractal dimension,[21] which is equivalent to a weaker decay of the scattering intensity when the scattering angle is increased. Apparently this effect is approximately included in the fitted *C*-parameter of eq 1, which is now larger than expected from the branching probability alone. Attempts to separate the excluded volume and the branching effect in *C* have not been successful so far.

In conclusion it can be said that a sensible but still only qualitative explanation can be given for the large difference in the branching probability determined from different molecular parameters which depend on this branching probability. The branching heterogeneity has

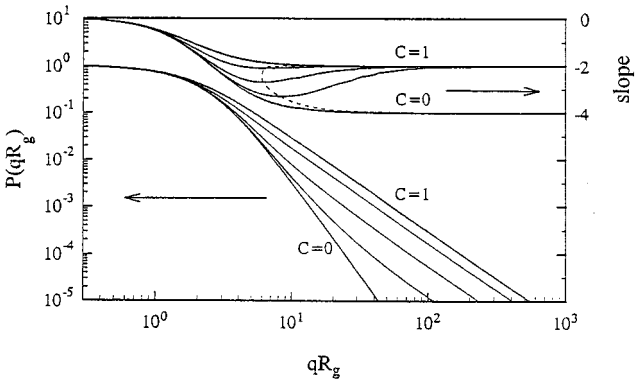

Figure 6. Double logarithmic plot of predicted particle scattering factors (lower part) and of the slopes at these curves (upper part). The slopes become constant at $qR_g > 80$ and approach a value of -2.00 for all examples, with the exception of $C = 0$, where the slope arrives at a value of -4.00.

undoubtedly a significant effect, but the largest influence certainly results from the excluded volume interaction that so far could not be incorporated into a suitable theory on branched macromolecules.

Are the Amylopectin Fractions Fractal Objects? At this point the question arises whether the slopes in Figure 3 really represent fractal behavior. In the beginning of this discussion we made the statement that the various starch fractions are not self-similar to each other. This is to say, the properties cannot universally be scaled. Still each fraction could have a self-similar *internal* structure, and in this case each molar mass may still be considered as a fractal object. The well developed power law dependencies of the scattering intensities seem to support this idea.

However, a more detailed analysis of the theoretical scattering curves discloses an effect that is demonstrated in Figure 6. Here the theoretically derived[13] angular dependencies of the particle scattering factor according to eq 1 are shown in the double logarithmic plot for fractions with the same branching probability but increasing molar mass, i.e. decreasing C-parameter. Up to the experimentally covered region of $qR_g = 8$ one may get the impression that the power law is reached. However, at larger values of qR_g the curves flatten again and eventually approach a slope of -2.00 that would be characteristic of linear chains in the unperturbed state.[21] Indeed, in this asymptotic region the window of observation is already sufficiently narrow that only the linear chain sections are seen. A large group of them are nonbranched outer chains. Hence, only in an intermediate q-region, corresponding to a volume that encompasses several branching generations, may the concept of fractal behavior be applied.[21] On the whole, however, these hyperbranched structures are not simple fractals, because the negative slope of the particle scattering factor continuously changes with the magnitude of the qR_g parameter (upper part of Figure 6). Actually according to the hyperbranching theory[13] only in a q-domain less than one decade may some sort of fractal behavior be observed. Table 2 gives a list of the asymptotic slope at $qR_g = 8$ in comparison to the calculated ones corresponding to the parameter C found from the fit of the experimental curve; the maximum slope that theoretically can occur[13] is also added. The positions of the maximum slopes are indicated by the dashed line in the inset of Figure 6.

A qualitative explanation can now be given for the apparently low branching probability that results from the fit parameter C. As already mentioned, the excluded volume causes a perturbation of the ideal Gaussian behavior only for the essentially nonbranched shells of outer chains which is the region of $qR_g > 10$. In this region we should observe a slope of -1.67, corresponding to the fractal dimension of a linear chain in a good solvent, which is $d_f = {}^5/_3$, while for the unperturbed chains the fractal dimension would be $d_f = 2.00$.[12,21] Thus, in the asymptotic region of $qR_g > 10$, a considerably weaker decay will result from the excluded volume. At smaller values of qR_g this asymptotically decaying tail will have some influence on the observed slope and will increase the C-parameter to the actually observed one. (See Figure 6).

Semidilute Concentration Regime. *Some General Relationships.* In the semidilute concentration regime the macromolecules are already fairly densely packed and interpenetrate each other at least partially. Intermolecular interactions now exert a dominating influence on the solution properties. Before entering this widely unexplored field, it may be helpful to recall in which manner most of the measurable quantities are affected by the intermolecular interactions at finite concentrations. One quantity that can be directly obtained is the ratio

$$\left(\frac{Kc}{R_{\theta=0}}\right)_c = \frac{1}{M_w}[1 + 2A_2M_wc + 3A_3M_wc^2 \ldots] \equiv \frac{1}{M_{app}(c)} \tag{4}$$

in which K is the usual optical contrast factor. Thus, actually only an apparent, concentration dependent molar mass $M_{app}(c)$ is obtained from the forward scattering intensity $R_{\theta=0}$. The effect of the repulsive interactions is represented by the terms in the square brackets.[22]

Furthermore, a distance length ξ or a radius of gyration R_g can be determined in any case from the initial part of the inverse scattering intensity as a function of q.[2]

$$R^2_{g,app}(c) \equiv 3\frac{\text{initial slope}}{\text{intercept}} \equiv 3\xi^2(c) \tag{5}$$

These dimensions are in general concentration dependent. The so-defined radius of gyration is an apparent one, as it does not represent the real dimension of the particle at the considered finite concentration. It is influenced by the intermolecular interactions, as will now be shown. Often the parameter ξ is used,[23] which denotes a not further specified correlation length. We prefer to keep the factor 3 in eq 5, since then the correct radius of gyration is obtained when the data are extrapolated to zero concentration.

To describe the influence of the intermolecular interactions, we use two approaches, which are appropriate for concentrations up to c^* and for much larger concentrations than c^*, respectively.

$c < c^*$. The starting point for the first approach results from the single-contact approximation of Zimm[24] that was extended to higher concentrations by Benoit et al.[25,26]

$$\frac{Kc}{R_\theta} = \frac{1}{M_wP(q)} + 2A_2c + \ldots \tag{6}$$

After expanding the particle scattering factor and collecting terms of q^2, one obtains

$$\frac{1}{M_w} + \frac{1}{3}\frac{R_g^2}{M_w}q^2 + 2A_2c \ldots = \frac{1}{M_{app}(c)} + \frac{1}{3}\frac{R_{g,app}^2}{M_{app}(c)}q^2 + \ldots \quad (7)$$

and

$$R_{g,app}^2(c) \cong R_g^2\frac{M_{app}(c)}{M_w} = \frac{R_g^2}{[1 + 2A_2M_wc + \ldots]} \quad (8)$$

where $R_{g,app}^2/M_{app}(c)$ is the initial slope of the angular dependent curve at concentration c, and the apparent molar mass $M_{app}(c)$ within the single contact approximation[24] is

$$\frac{1}{M_{app}(c)} = \frac{1}{RT}\frac{\partial\pi}{\partial c} \cong \frac{1}{M_w} + 2A_2c + \ldots \quad (9)$$

$c \gg c^*$. It is tempting to apply eq 8 also to higher concentrations where higher virial coefficients have to be taken into account. The validity of this attempt may be expected up to the overlap concentration but not in the typical semidilute regime where $c/c^* \gg 1$. In this region the correlation length $\xi \equiv (1/3)^{1/2}R_{g,app}$ should be independent of the molar mass and solely dependent on the concentration.[23]

As for linear, flexible chains we may assume also for branched structures scaling behavior of the type[23]

$$R_{g,app}(c) = R_g(c/c^*)^m \quad (10)$$

with an exponent m yet to be determined. The radius of gyration at infinite dilution, R_g, has a molar mass dependence that obeyed power law behavior[1] with an exponent of $\nu = 0.39 \pm 0.01$. For the overlap concentration we use the definition via the second virial coefficient[22,27]

$$c^*_{A_2} = (A_2M_w)^{-1} \quad (11)$$

which gives

$$c/c^*_{A_2} = A_2M_wc = X \quad (12)$$

The second virial coefficient A_2 also followed a power law dependence on the molar mass[2] but with a much larger negative exponent of $a_{A_2} = -0.61 \pm 0.02$ for the amylopectin fractions[2] than known for linear chains with $a_{A_2} = -0.2$. This molar mass dependence causes a power law behavior also for $1/c^* \propto M^{(1+a_{A_2})}$. The condition of molar mass independence of the apparent radius of gyration then leads to the relationship

$$\nu + (1 + a_{A_2})m = 0 \quad (13)$$

With the experimental data of $\nu = 0.39 \pm 0.01$ and $a_{A_2} = -0.61 \pm 0.02$ one obtains

$$m = -1.00 \pm 0.03 \quad (14)$$

Hence asymptotically a decrease of $R_{g,app}(c)$ as c^{-1} should be observed for these branched samples instead of the weaker decrease with exponent $m = -3/4$ for linear chains.[23] This behavior should be the same for all amylopectin samples.

Experimental Findings. The scattering data obtained at different concentrations are mostly represented in a Zimm plot[24] or equivalent modifications of this.[17] The different curves then are extrapolated to zero scattering angle and, for each scattering angle, to concentration $c = 0$. This procedure leads to two limiting curves: (i) the angular dependence at $c = 0$ results from the scattering behavior of individual chains with no intermolecular interactions; (ii) the other at $q = 0$, represents the intermolecular interactions that are not influenced by interference effects resulting from the size of the particles. Both limiting curves could be conclusively interpreted.[2] For illustration such a plot is shown in Figure 7, here in the Berry representation.[17,28] This procedure neglects the whole area of scattering data which are spanned by these two limiting curves. We now deal with this so far unexplored region of finite q and finite concentration c, and we wondered whether this region could be deduced if the two limiting curves are known. This idea proved to be applicable.

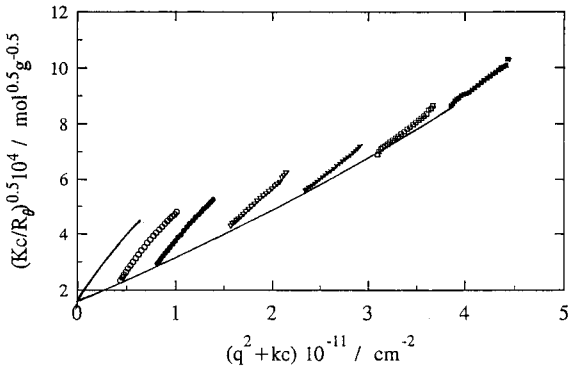

Figure 7. Berry plot of the light-scattering data from *LD18* at 6 concentrations in the range from $c_1 = 1.3$ mg/mL to $c_6 = 12.7$ mg/mL. The overlap concentration is $c^*_{A_2} = 2.8$ mg/mL, which is slightly higher than c_2.

Figure 7 shows the measurements of $(Kc/R_\theta)^{1/2}$ (Berry plot) from six concentrations in the range from $c = 1.3 \times 10^{-3}$ to 12.7×10^{-3} g/cm^3, and Figure 8 represents the concentration dependence of the apparent and true radius of gyration at concentration c that was calculated with eq 8. The overlap concentration of the sample was $c^*_{A_2} = (A_2M_w)^{-1} = 2.8$ g/cm^3.

Discussion

Concentration Dependence of $R_{g,app}(c)$. The correction of eq 8 gave a radius of gyration R_g that remained unchanged up to about $c \cong c^*$. Thereafter an increase becomes noticeable which has to be considered as incorrect. As already mentioned eq 8 can be correct only if $c < c^*$. For $c \gg c^*$ the approximation of eq 10 has to be applied. The apparent mean square radius of gyration was predicted to decrease with c^{-1} (eq 14). This behavior is indeed observed, as is shown in Figure 8a. In this region of $c >> c^*$ the approximation of eq 8 overestimates the correction, since the apparent molar mass decreases more strongly with increasing concentration (approximately with $c^{-1.25}$) than the apparent mean square radius. This causes an increase of the calculated radius $R_g(c)$ that actually results from the invalidity of this approximation when $c > c^*$ (see Figure 8b). At $c \gg c^*$ a drastic increase of the radius $R_g(c)$ with the concentration is obtained. This effect results from association, which was confirmed by an increase of the corrected molar mass $M_w(c)$ at the same concentrations as was already outlined in paper 2.[2]

Scaling of the Angular Dependence. As for infinitely dilute solutions a dimensionless apparent particle scattering factor can be defined also for finite concentrations

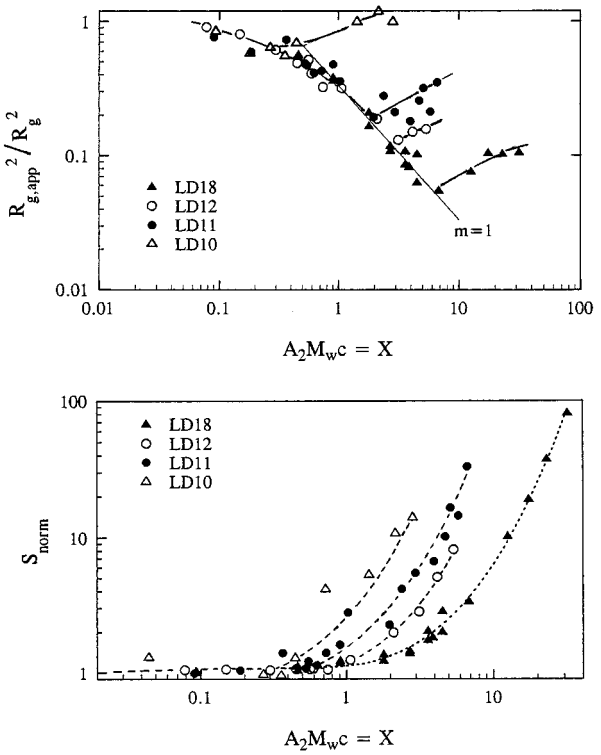

Figure 8. (a, top) Concentration dependence of the apparent mean square radii of gyration for four LD*X* samples. The slope $m = -1$ is predicted from eq 13. The sharp increase beyond a certain concentration indicates cluster growth due to association. The onset of association is shifted to lower $c/c^*_{A_2}$ for the samples with lower molar mass. (b, bottom) The same data after correction due to eq 7. $S_{norm} = (R^2_{g,app}/R^2_g)(M_w/M_{app})$.

$$P_{app}(q,c) \equiv \frac{S(q,c)}{S(q=0,c)} \qquad (15)$$

where $S(q,c)$ is the structure factor and $S(q=0,c) = RT(\partial c/\partial\pi)$ is the corresponding value at scattering angle $\theta = 0$ (forward scattering). Because of the different curvatures it appeared at first sight to be unlikely that the six curves of Figure 9a could be cast into one master curve. However, when plotting $P_{app}(q,c)$ against $qR_{g,app}(c)$ all curves collapse to one master curve which is identical with that at infinite dilution. The result is shown in Figure 9b. This behavior allows the conclusion that the *shape* of the macromolecule is not changed by the thermodynamic intermolecular interaction. Thus, once the two limiting scattering curves at $c = 0$ and $\theta = 0$ are known, the whole set of data can exhaustively be described. This statement remains true, of course, only as long as association phenomena are not effective.

Conclusions

It is evident that when the polymer concentration is increased also the repulsion among the branched particles is increased. It appeared conceivable to us that the repulsive force, in particular at concentrations well above the overlap concentration, would have an effect on the particle scattering factor and the dimensions of the molecules. This, however, was not observed; the apparent particle scattering factor remained unchanged and showed the same angular dependence as the curve at $c = 0$, when the apparent radius of gyration is used as a scaling factor. The highest concentration in this example was about 5 times the overlap concentration.

In branched polymers only the shells of chains at the outside can interpenetrate. For the sample LD*18* this

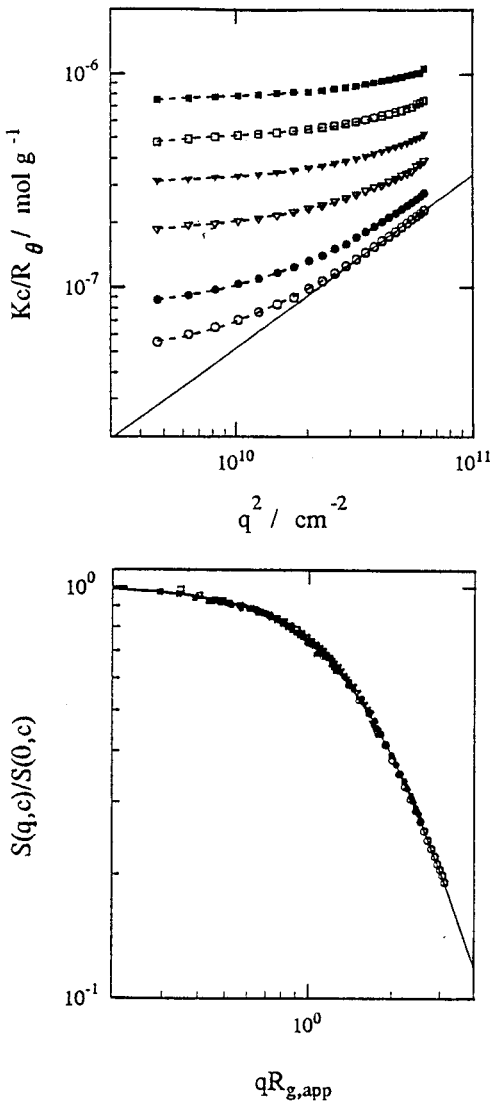

Figure 9. (a, top) Plot of the reciprocal scattering intensity against q^2 for the six concentrations of LD*18* from Figure 7. (b, bottom) Same data but now normalized by the forward scattering intensity and plotted against $qR_{g,app}$. The full line corresponds to the curve at $c = 0$.

still seems to be the case up to $c/c^* \approx 5$. At $c/c^* > 10$, however, association starts. The swollen particles cannot penetrate deeper and have now to be compressed to a smaller volume. The local segment concentration is increased, and thus the probability of forming hydrogen bonds between the segments of the different particles increases. Figure 10 shows the effect of association with the sample LD*11* (M_w = 830 000 g/mol). Association occurs at about $c/c^* > 7$, where $c^* = 10.8$ g/cm^3. The beginning of association is clearly detected when plotting the apparent radius of gyration $R_{g,app}(c)$, or with eq 8 corrected radius $R_g(c)$, against the concentration, as is shown in Figure 8. The former passes through a sharp minimum and then increases strongly, while the "corrected" ones remain almost constant up to $c = c^*$ and increase sharply beyond the concentration where $R_{g,app}(c)$ has its minimum. As already outlined, the increase is somewhat overestimated in eq 8 as the repulsive interactions have a weaker influence on $R^2_{g,app}(c)$ than on the apparent molar mass. Since the apparent molar mass of the associated particles also increases, we are not able to judge in which manner the shape of the individual molecules is changed as a result of association. What was observed in the region of

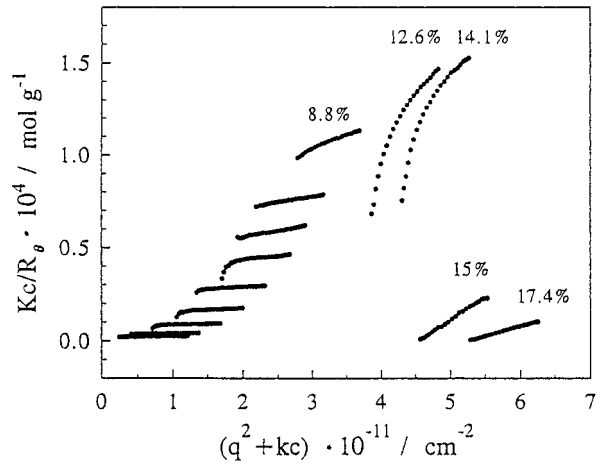

Figure 10. Zimm plot of the LD*11* data measured in a wide concentration range. The overlap concentration is $c^*_{A_2} = 1.08\%$, which corresponds to the third curve. Association becomes noticeable at $c/c^*_{A_2} > 3$ and dominates at $c/c^*_{A_2} > 7$.

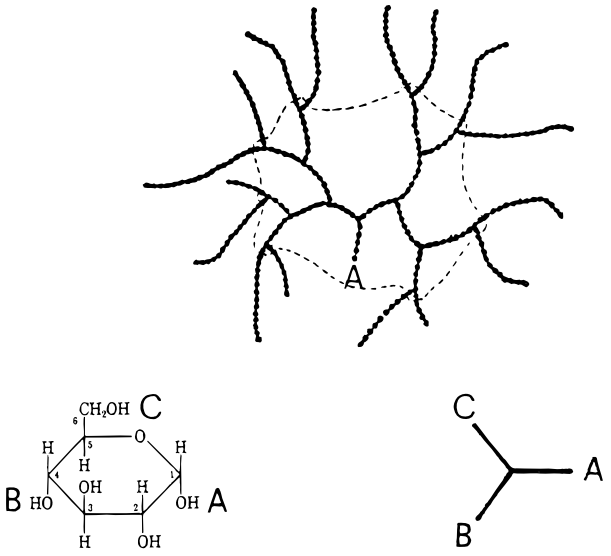

Figure 11. Functional groups of the glucose units in amylopectin and the structure resulting from the $A\text{-}\langle{}^{C}_{B}$-polycondensation in which A can react only with B or C.

association is a relationship of

$$R_{g,app}(c) \sim M_{app}(c)^{2.6\pm0.2} \tag{16}$$

An exponent of 2.5 is characteristic for a random cluster−cluster association of nonswollen particles.[2,12,21] Equation 16 is at the present stage solely an empirical relationship, and conclusions have to be made with caution.

Acknowledgment. The authors thank the Deutsche Forschungsgemeinschaft for supporting this study.

Appendix: Some Relationships of the $A\text{-}\langle{}^{C}_{B}$-Polycondensation Model[13]

The model goes back to Flory[3] and more specifically to calculations by Erlander and French.[29] Further derivations concerning the mean square radius of gyration, the hydrodynamic radius and the particle scattering factor were made by one of the present authors.[13] Figure 11 shows a glucose unit and the assignment of the reactive groups A, B, and C to the OH groups at the C1 (reducing end group), C_4, and C_6 positions of the glucose ring. Because of enzymatic specificity bonds can be formed only between $C_1 \rightarrow C_4$ and $C_1 \rightarrow C_6$; all other reactions are excluded. The corresponding extents of reaction (probability of reaction) are p_1, p_4, and p_6 with the obvious constraint

$$p_1 = p_4 + p_6 \tag{A1}$$

This model corresponds to the general case of hyperbranching and reduces to the *common hyperbranching process* for

$$p_4 = p_6 = \frac{p_1}{2} \tag{A2}$$

In amylopectin and glycogen $p_6 = p$ is the branching probability, which does not depend on the molar mass of the branched polysaccharides.

According to the common (mean field) theory of branching processes, one has for the

$$M_n = \frac{162}{1 - p_1} \tag{A3}$$

$$M_w = 162\frac{1 - p_4^2 - p^2}{(1 - p_4 - p)^2} \tag{A4}$$

$$\begin{aligned} M_z = 162\{&[(1 - p_1)(1 - p_4^2 - p^2) - \\ &2(1 - p_1)[p_4^2(1 - p_4) + p^2(1 - p)] + \\ &3(1 - p_4^2 - p^2)[p_4(1 - p_4) + p(1 - p)]]/ \\ &[(1 - p_1)^2(1 - p_4^2 - p^2)]\} \end{aligned} \tag{A5}$$

$$\frac{M_w}{M_n} = 1 + [1 + 2p(1 - p)DP_w]^{1/2} = 2(1 + B_n) \tag{A6}$$

$$B_n = p(1 - p)DP_n$$

$$\frac{R_g}{R_h} \equiv \rho = \left(\frac{3(1 + 2B_n)}{4(1 + B_n)}\right)^{0.5}\left(\frac{2 + B_n}{1 + B_n}\right) \tag{A7}$$

$$C_h = \frac{1}{6}\frac{1 + B_n}{1 + 2B_n}\left(1 + \frac{1}{5}\frac{2 + 3B_n}{2 + B_n} + \frac{B_n}{(1 + 2B_n)(2 + B_n)}\right) \tag{A8}$$

where

$$B_n = p(1 - p)DP_n$$

$$B_w = p(1 - p)DP_w \tag{A9}$$

$$D_{app}(q) = D_z(1 + C_h R_g^2 q^2 - ...) \tag{A10}$$

Particle Scattering Factor

$$P_z(q) = \frac{1 + \frac{C}{3}R_g^2 q^2}{\left[1 + \frac{1 + C}{6}R_g^2 q^2\right]^2} \tag{A11}$$

with

$$C = \frac{p_4^2 + p^2}{p_1 + \frac{2pp_4}{1 - p_1}} \tag{A12}$$

References and Notes

(1) Galinsky, G.; Burchard, W. *Macromolecules* **1995**, *28*, 2363.
(2) Galinsky, G.; Burchard, W. *Macromolecules* **1996**, *29*, 1498.
(3) Flory, P. J. *Principles of Polymer Chemistry*; Cornell University Press: Ithaca, NY, 1953.
(4) Guilbot, A.; Mercier, Ch. Starch. In *The polysaccharides*; Aspinall, G. O., Ed.; Academic Press: London, 1985; Vol. 3.
(5) Robin, J. P.; Mercier, Ch.; Duprat, F.; Charbonniere, R.; Guilbot, A. *Starch/Stärke* **1975**, *7*, 36.
(6) Fox, J. A.; Robyt, J. F. *Carbohydr. Res.* **1992**, *227*, 163.
(7) Jenkins, P. J.; Cameron, R. E.; Donald, A. M.; Bras, W.; Derbyshire, G. E.; Mant, G. R.; Ryan, A. J. *J. Polym. Sci., Polym. Phys. Ed.* **1994**, *32*, 1579.
(8) Jenkins, P. J.; Donald, A. M. *Int. J. Biol. Macromol.* **1995**, *17*, 315.
(9) Bantle, S.; Schmidt, M.; Burchard, W. *Macromolecules* **1988**, *15*, 1604.
(10) Trappe, V.; Bauer, J.; Weissmüller, M.; Burchard, W. *Macromolecules* **1997**, *30*, 2365.
(11) Stanley, H. E. *Introduction to Phase Transitions and Critical Phenomena;* Clarendon Press: Oxford, 1971.
(12) Stauffer, D. *Introduction to Percolation Theory*; Taylor & Francis: Philadelphia, PA, 1985.
(13) Burchard, W. *Macromolecules* **1977**, *10*, 919.
(14) Zimm, B. H.; Stockmayer, W. H. *J. Chem. Phys.* **1949**, *17*, 1301.
(15) Whistler, R. L., BeMiller, E.; Paschall, E. F. Eds. *Starch: Chemistry and Technology*; Academic Press: New York, 1984.
(16) Thurn, A.; Burchard, W. *Carbohydr. Polym.* **1985**, *5*, 441.
(17) Burchard, W. *Adv. Polym. Sci.* **1983**, *48*, 1.
(18) Equation 2 agrees almost perfectly with the corresponding relationship derived by Zimm and Stockmayer[14] for randomly branched clusters of uniform molar mass.
(19) Daoud, M.; Cotton, J. P. *J. Phys. (Paris)* **1982**, *43*, 531.
(20) Huber, K.; Burchard, W.; Fetters, L. J. *Macromolecules* **1984**, *17*, 541.
(21) Daoud, M.; Martin, J. E. Fractal Properties of Polymers. In *The Fractal Approach to Heterogeneous Chemistry*; Avenir, D., Ed.; Wiley: New York, 1992.
(22) Burchard, W.; Lang, P.; Schulz, L.; Coviello, T. *Macromol. Symp.* **1992**, *58*, 21.
(23) De Gennes, P.-G. *Scaling Concepts in Polymer Physics*; Cornell University Press: Ithaca, NY, 1979.
(24) Zimm, B. H. *J. Chem. Phys.* **1948**, *16*, 1093.
(25) Benoit, H.; Benmouna, M. *Polymer* **1984**, *25*, 1059.
(26) Benoit, H.; Higgins, J. S. *Polymers and Neutron Scattering*; Clarendon Press: Oxford, 1994.
(27) Freed, K. F. *Renormalization Group Theory of Macromolecules*; Wiley: New York, 1987.
(28) Berry, G. C. *J. Chem. Phys.* **1966**, *44*, 4550.
(29) Erlander, S.; French, D. *J. Polym. Sci.* **1956**, *20*, 7.

MA961775O